

FLAT ELECTRON BUNCH COMPRESSION AT THE ADVANCED SUPERCONDUCTING TEST ACCELERATOR

P. Piot^{1,2}, C. R. Prokop¹, B. E. Carlsten³, D. Mihalcea¹, Y.-E. Sun⁴

¹ Department of Physics, Northern Illinois University DeKalb, IL 60115, USA

² Fermi National Accelerator Laboratory, Batavia, IL 60510, USA

³ Los Alamos National Laboratory, Los Alamos, NM, 87544 USA

⁴ Argonne National Laboratory, Argonne, IL 60439, USA

The generation of flat beam using round-to-flat beam conversion of an incoming canonical-angular-momentum dominated electron beam could have important application in the field of advanced acceleration techniques and accelerator-based light source. In this paper we explore the temporal compression of flat beams and especially compare the resulting phase space dilutions with the case of round beam. Finally, we propose and detail a possible experiment to investigate the flat-beam bunch compression at the Advanced Superconducting Test Accelerator currently in construction at Fermilab.

I. INTRODUCTION

An important asset of the ASTA photoinjector [1] is its capability to generate beams with high-transverse emittance ratios known as flat beams. Immersing the photocathode in a magnetic field introduces a canonical angular momentum $\langle L \rangle = eB_0\sigma_c^2$, with B_0 the magnetic field on the photocathode surface, and σ_c the RMS transverse size of the drive-laser spot on the photocathode [2]. As the beam exits the solenoidal field the angular momentum is purely kinetic resulting in a beam coupled in the two transverse planes. The transverse eigen-emittances (the eigenvalues of the beam matrix) are not degenerated. Three skew quadrupoles in the beamline can apply the torque necessary to cancel the angular momentum [3, 4]. In this process the final beam's transverse emittances, downstream of the round-to-flat-beam (RFTB) converter, equates the eigen-emittances [3]

$$(\varepsilon_{x,i}, \varepsilon_{y,i}) = \left(2\beta\gamma\mathcal{L}, \frac{\varepsilon_u^2}{2\beta\gamma\mathcal{L}} \right), \quad (1)$$

where ε_u is the normalized uncorrelated emittance of the magnetized beam prior to the transformer, β and γ the Lorentz factors, $\mathcal{L} \equiv \langle L \rangle / 2p_z$, and p_z is the longitudinal momentum. Note that the product $\varepsilon_{x,i}\varepsilon_{y,i} = (\varepsilon_u)^2$. In our notations, the smaller emittance is associated to the vertical direction and the emittance ratio $\rho \equiv \varepsilon_{x,i}/\varepsilon_{y,i} > 1$. If compressed these flat beams may have applications in Smith-Purcell FELs [5] or for beam-driven acceleration techniques using asymmetric structures [6]. It may also be possible to mitigate the bending-plane emittance growth in the bunch compressor [7]. Finally, when combined with transverse-to-longitudinal emittance-exchange techniques, the RFTB method enables repartitioning of the beam emittance within the three degrees of freedom.

II. FLAT-BEAM GENERATION

A description of the ASTA photoinjector and its performances associated to round beams generation is presented in Ref. [1]; see Fig. 1. The electron source includes of a 1.3-GHz 1+1/2 radiofrequency (rf) gun [8] surrounded by two solenoids. The generated beam is then injected in two superconducting rf (SRF) cavities and accelerated up to 50 MeV. A set of three skew quadrupoles (RFTB in Fig. 1) located downstream of the accelerating section can be used to transform an angular-momentum-dominated beam into a flat beam. The flat beam can be compressed using a chicane bunch compressor (BC1) and either send to a user beamline or further accelerated. The longitudinal dispersion of BC1 is $R_{56} = -0.19$ m. A third SRF cavity (CAV39) operating at 3.9 GHz will eventually be incorporated to correct for nonlinear longitudinal phase space distortions.

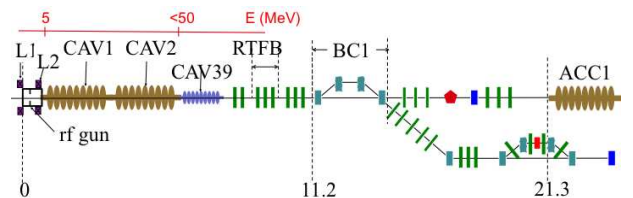


FIG. 1: Overview of the ASTA photoinjector. The legend is as follows "L1" and "L2" are solenoids, "CAV1", "CAV2" and "CAV39" are SRF accelerating cavities, "RFTB" is the round-to-flat beam, "BC1" is a magnetic-chicane bunch compressor and "ACC1" is the first accelerating cryomodule. The distances (in meters) shown at the bottom are referenced to the cathode surface.

In order to optimize the performance of the flat-beam generation we improve the methods previously introduced [9]. We take the particle coordinates in the transverse trace spaces to be $\tilde{\mathbf{X}} \equiv (x, x')$ and $\tilde{\mathbf{Y}} \equiv (y, y')$ where x and x' are the position and divergence coordinates and $\tilde{\cdot}$ is the transpose operator. We introduce the correlation matrix such that $\mathbf{Y} = \mathbf{C}\mathbf{X}$ and statistically

extend its definition to $C \equiv \langle \mathbf{Y}\tilde{\mathbf{X}} \rangle \langle \mathbf{X}\tilde{\mathbf{X}} \rangle^{-1}$ where $\langle \mathbf{X}\tilde{\mathbf{X}} \rangle$ and $\langle \mathbf{Y}\tilde{\mathbf{X}} \rangle$ are 2×2 blocks of the 4D beam matrix Σ . The form of the correlation matrix is constraints and can be shown to be $C_{2,1} = -(1 + a^2)/b$ where $a \equiv C_{1,1} = -C_{2,2}$ and $b \equiv C_{1,2}$ which insures $|C| = 1$ [9]. Upon knowledge of the incoming C matrix downstream of CAV39, the RFTB is tuned to apply the necessary torque to insure all the elements of C identically vanish downstream of the RFTB [3, 9]. Considering the RFTB configuration implemented at ASTA (three skew quadrupole with 0.167 m effective length separated by 0.38 m) and limited strengths (typically $k_1 \leq 30 \text{ m}^{-2}$), flat beam generation is only possible for a limited values of the parameters a and b associated to the incoming correlation matrix; see Fig. 2.

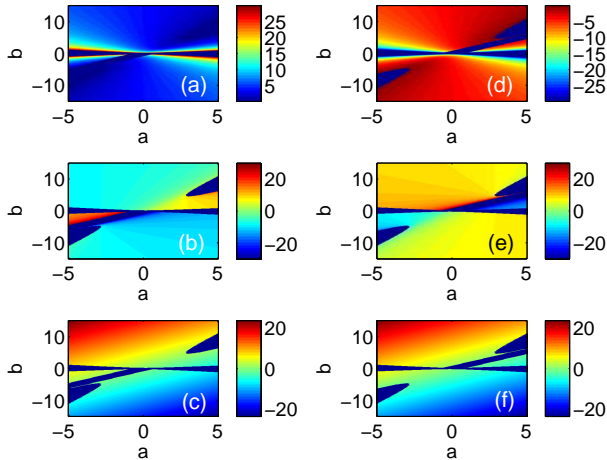


FIG. 2: Required strength for the 3 skew quadrupoles used in the RFTB [quadrupoles 1, 2, 3 are respectively shown in plots (a), (b) and (c) or (d), (e), and (f)]. The right and left columns respectively corresponds to the two possible solutions for the quadrupole settings [10].

The optimization of the flat beam production consists in first optimizing the photoinjector settings (solenoid field, photocathode laser spot size) such to minimize the 4D emittance $\varepsilon_{4D} \equiv |\Sigma|^{1/4}$ downstream of the accelerating section. The simulation were performed with ASTRA [11] and a multi-objective optimizer [12]. Beside minimizing the 4D emittance a second objective was to maximize the emittance ratio computed as the ratio of the achieved eigen emittances. Figure 3 displays the evolution of the 4D emittance and emittance ratio for an optimized case with parameter listed in Tab. I. We confirmed that the 4D emittance after optimization of the flat beam configuration attained a value similar to the round-beam configuration simulated in Ref. [1]; see Tab. I.

TABLE I: Comparison of achieved beam parameter for the round- and flat-beam configuration.

parameter	flat-beam configuration	round-beam configuration	units
Q	3.2	3.2	nC
E	47.18	48.77	MeV
ε_x	105.04	5.43	μm
ε_y	0.31	5.44	μm
ε_{4D}	5.53	5.44	μm
ρ	$\simeq 334$	$\simeq 1$	—

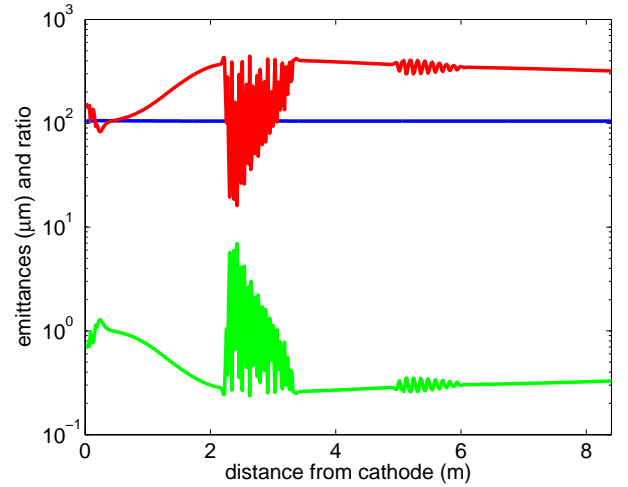


FIG. 3: Evolution of the eigen-emittance (green and blue traces) and associated ratio (red) along the photoinjector. The ordinate $z = 8.5 \text{ m}$ corresponds to the exit of CAV39.

III. FLAT-BEAM COMPRESSION

Downstream of the RFTB, the bunch can be shortened in the BC1 compressor. Introducing the longitudinal phase space (LPS) chirp as $\mathcal{C} \equiv -\langle z\delta \rangle / \langle z^2 \rangle$ [where (z, δ) is the longitudinal position and relative momentum offset of the particles], maximum compression occurs at $\mathcal{C} = -1/R_{56} \simeq 5.2 \text{ m}^{-1}$.

Two major issues arise when compressing a flat beam. Since the RFTB is located between the accelerating section and BC1, the beam dynamics during the flat-beam transformation might be subject to larger fractional momentum spread (as the linac need to impact a correlated energy spread for compression in BC1). Second, the beam dynamics of the flat beam during compression need to be investigated.

In order to explore the behavior of flat beams in the BC1 compressor as a function of initial emittance ratios ρ , we took particle distribution associated to a 3.2 nC bunch and numerically scaled the macroparticle coordinates to produce the desired transverse emittance ratios while constraining the product $\varepsilon_{x,i}\varepsilon_{y,i} = 5^2 \mu\text{m}^2$ to be

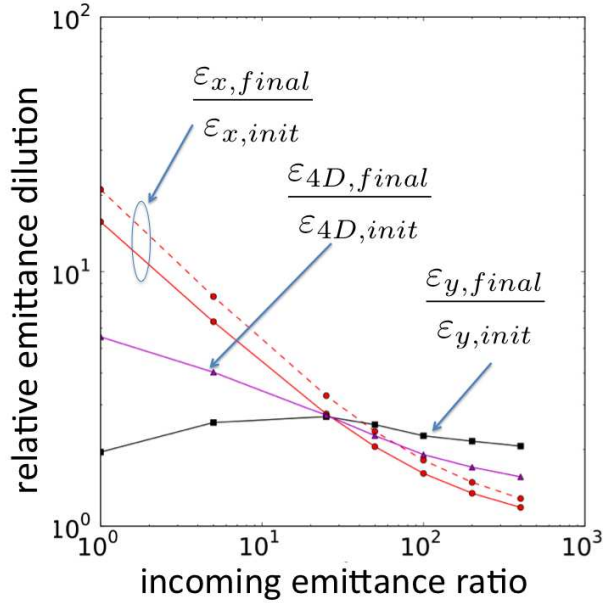


FIG. 4: Bending plane transverse-horizontal emittance growth in BC1 (red traces) simulated with CSRTRACK (dashed line) and IMPACT-Z (solid lines) as functions of the initial transverse emittance ratio. Corresponding IMPACT-Z results for the vertical emittance (black line), and 4D emittance (magenta).

consistent with the achieved 4D emittance. The simulations are carried with IMPACT-Z [13] and CSRTRACK [14]. The former program simulates CSR using a 1D model (projected model) while the latter program has a more precise but CPU-demanding point-to-point (P2P) algorithm. The one-dimensional model is valid provided [15]

$$\mathcal{D}(s) \ll 1, \text{ with } \mathcal{D}(s) \equiv \frac{\sigma_x(s)}{\sigma_z(s)} \sqrt{\frac{\sigma_x(s)}{R(s)}}, \quad (2)$$

where $R(s)$ is the trajectory's radius of curvature and $\sigma_x(s)$ and $\sigma_z(s)$ are respectively the transverse and longitudinal root-mean-square (RMS) sizes at the curvilinear beamline position s .

Due to the large transverse aspect ratio of the bunches, it is anticipated that the projected CSR model used in IMPACT-Z is inadequate, thus we use CSRTRACK's P2P model to simulate the flat beams dynamics throughout BC1. The parameters used for flat beam simulations follow those used in the previous section, with the exception of the macroparticle horizontal size use in the CSRTRACK P2P model. Due to the much greater transverse dimension we set the horizontal size of the Gaussian macroparticles used in the P2P algorithm to $\sigma_h = 0.2$ mm. In addition, IMPACT-Z simulations were also carried to evaluate the emittance growth in the vertical plan. The simulated emittance growth is shown in Fig. 4 for a 3.2-nC bunch with an initial LPS chirp of $\mathcal{C} = 5.2$ m⁻¹. As expected the relative emittance dilution is reduced as the initial emittance ratio ρ increases. The agreement between CSRTRACK and IMPACT-Z for the bending-plane emittance dilution is remarkable (within ~ 30 %) given the large transverse horizontal beam sizes. In addition, IMPACT-Z predicts that the vertical emittance increases by a factor 1.5 to 1.8 over the range of considered initial emittance ratios $\rho \in [1, 500]$. We also observe that the 4D emittance growth is mitigated for the larger initial flat-beam emittance ratios [7].

[1] P. Piot, et al, Proc. IPAC10, 4316 (2010).
 [2] R. Brinkmann, et al. PRSTAB **4**, 053501 (2001).
 [3] K.-J. Kim, PRSTAB **6**, 104002 (2003).
 [4] P. Piot, et al., PRSTAB **9**, 031001 (2006).
 [5] C. Prokop, et al. APL **96**, 151502 (2010).
 [6] D. Mihalcea, et al., PRSTAB **15**, 081304 (2012).
 [7] C. Prokop, et al., NIMA **719**, 18 (2013).
 [8] B. Dwersteg, et al., NIMA **393**, 93 (1997).
 [9] E. Thrane, et al., Proc. LINAC02, 308 (2002).

[10] Y.-E Sun, et al, Proc. LINAC04, 378 (2004).
 [11] K. Flöttmann, ASTRA user manual, DESY (2000).
 [12] H. Shang, M. Borland, GeneticOptimizer, private communication (2007).
 [13] J. Qiang, et al., J. Comp. Phys. **163**, p. 434 (2000).
 [14] M. D. Dohlus et al., Proc. FEL04. 18 (2004).
 [15] Ya. S. Derbenev and V. D. Shiltsev. SLAC-PUB-7181, (1996).